Adsorption (2012) 18:445–459
DOI 10.1007/s10450-012-9431-1

CO_2 capture from flue gas by two successive VPSA units using 13XAPG

Lu Wang · Zhen Liu · Ping Li · Jin Wang · Jianguo Yu

Received: 22 May 2012 / Accepted: 17 September 2012 / Published online: 5 October 2012

Abstract With the development of novel adsorbent material and adsorption process, adsorption technology has become a potential tool for the CO_2 removal from flue gases. The reduction of carbon dioxide emissions from flue gases with two successive vacuum pressure swing adsorption (VPSA) units, using 13XAPG as the adsorbent, was investigated both theoretically and experimentally. A 3-bed 5-step VPSA process was designed to capture CO_2 from flue gases, which included feed pressurization, adsorption, rinse, blowdown and counter-current purge. It was found that was difficult to achieve both high CO_2 purity and high CO_2 recovery by one VPSA unit when capturing CO_2 from flue gases at atmospheric pressure. After the verification of one-column VPSA experiment for further concentrating CO_2 stream from one VPSA unit to above 95 % purity, two successive VPSA units were designed, composed of 3-bed 5-step cycle for the first unit and 2-bed 6-step cycle for the second unit, and the effects of operating parameters on the separation behaviors were investigated by simulation. With the proposed VPSA process, a CO_2 purity of 96.54 % was obtained with recovery of 93.35 %. The total specific power consumption of the two successive VPSA units was 528.39 kJ/kg_{CO_2}, while the unit productivity was 0.031 kg_{CO_2}/kg h.

Keywords CO_2 capture · Vacuum pressure swing adsorption · Zeolite 13X · Simulation · Two successive VPSA units

Nomenclature

a'	area-to-volume ratio, 1/m
a_i	number of neighboring sites occupied by a molecule of component i
Bi_i	Biot number of component i, calculated by $Bi_i = \frac{R_p k_{fi}}{5\varepsilon_p D_{p,i}}$
$\overline{C_i^p}$	averaged concentration in the macropores for component i, mol/m^3
C	concentration, mol/m^3
C_i	concentration of component i in the gas phase, mol/m^3
$C_{p,i}$	molar constant pressure specific heat of the gas mixture, J/mol K
C_p	molar constant pressure specific heat of the gas mixture, J/mol K
$C_{pgmass,i}$	mass constant pressure specific heat of the pure gas, J/kg K
C_{pgmass}	mass constant pressure specific heat of the gas mixture, J/kg K
C_{ps}	constant pressure specific heat of the adsorbent, J/kg K
C_{pw}	specific heat of the column wall, J/kg K
C_v	molar constant volumetric specific heat of the gas mixture, J/mol K
C_{vi}	molar constant volumetric specific heat of component i, J/mol K
$C_{v,ads,i}$	molar constant volumetric specific heat of component i adsorbed, J/mol K
C_t	total gas concentration, mol/m^3
d_p	pellet diameter, m
D_{ax}	axial dispersion coefficient, m^2/s
$D_{p,i}$	pore diffusivity of component i, m^2/s
$D_{m,i}$	molecular diffusivity of component i, m^2/s
$D_{k,i}$	Knudsen diffusivity of component i, m^2/s
D_w	internal diameter of the column, m
$D_{\mu,i}$	crystal diffusivity of component i, m^2/s

L. Wang · Z. Liu · P. Li (✉) · J. Wang · J. Yu
State Key Laboratory of Chemical Engineering, College of Chemical Engineering, East China University of Science and Technology, Shanghai 200237, China
e-mail: liping_2007@ecust.edu.cn

$D^0_{\mu,i}$	limiting diffusivity at infinite temperatures for component i, m^2/s
e	wall thickness, m
$E_{a,i}$	activation energy of microspore diffusion for component i, kJ/mol
h_f	film heat transfer coefficient between the gas and the solid phase, W/m^2 K
h_w	film heat transfer coefficient between the gas phase and the column wall, W/m^2 K
k_{fi}	film mass transfer coefficient, m/s
k_g	thermal conductivity of the gas mixture, W/m^2 K
k_i	thermal conductivity of component i, W/m^2 K
K_i	adsorption equilibrium constant of component i, 1/kPa
K^0_i	adsorption equilibrium constant at the limit $T \to \infty$ of component i, 1/kPa
L_c	column length, m
M_i	molecular weight for component i, g/mol
N	number of the cycle
Nu	Nusselt number
P	total pressure, Pa
P_{atm}	atmospheric pressure, Pa
$P_{cycleend}$	pressure at the beginning of pressurization step, Pa
P_{exit}	purge pressure at the feed end, Pa
P_{feed}	feed pressure, Pa
P_{high}	high pressure, Pa
P_{vacu}	low pressure, Pa
Pr	Prandtl number
q_{eq0,N_2}	adsorbed phase concentration of nitrogen at the initial stage, mol/kg
q_i	adsorbed phase concentration of component i, mol/kg
q^*_i	adsorbed gas-phase concentration in the equilibrium state of component i, mol/kg
$\overline{q_i}$	pellet averaged adsorbed phase concentration, mol/kg
$\langle\overline{q_i}\rangle$	adsorbed phase concentration of crystals averaged over the entire pellet, mol/kg
$q_{\max,i}$	saturation capacity of component i, mol/kg
r_c	radius of the crystal, m
r_p	radius of the pore, cm
R_c	radius of the column, m
Re	Reynolds number
r	radial distance coordinate in the crystal, m
R	radial distance coordinate in the pellet, m
R_p	radius of the pellet, m
R_g	universal gas constant, J/mol K
R_w	radius of the wall, m
Sc	Schmidt number
Sh	Sherwood number
t	time, s
t_{feed}	feed step time, s
t_{press}	pressurization step time, s
t_{vacu}	vacuum step time, s
t_{purge}	purge step time, s
t_{total}	cycle time, s
T	temperature, K
T_{feed}	feed temperature, K
T_g	temperature of the gas phase, K
T_s	temperature of the solid phase, K
T_w	wall temperature, K
T_∞	environment temperature, K
u	superficial velocity of component i, m/s
U	global external heat transfer coefficient, W/m^2 K
W_{ads}	weight of adsorbent, kg
y_i	molar fraction of component i
$y_{feed,i}$	molar fraction of feed gas for component i
$y_{initial,i}$	molar fraction of component i in the initial stage
z	axial distance along the column, m

Greek Letters

α_w	ratio of the internal surface area to the volume of the column wall, 1/m
α_{wl}	ratio of the logarithmic mean surface area of the column shell to the volume of the column wall, 1/m
γ	heat capacity ratio, represented by $\gamma = C_p/C_v$
ρ_b	gas density in the bulk, kg/m^3
ρ_c	column density, kg/m^3
ρ_g	gas density, kg/m^3
ρ_p	pellet density, kg/m^3
ρ_w	column wall density, kg/m^3
λ	axial heat dispersion, W/m^2 K
θ	parameters for pressure change during depressurization or vacuum
$(-\Delta H_i)$	isosteric heat of adsorption of component i, kJ/mol
ε_c	porosity of the column
ε_p	porosity of the pellet
τ_p	pellet tortuosity
μ_g	gas viscosity, Pa s

1 Introduction

Serious concerns have been raised with respect to the impact of the increasing concentration of carbon dioxide in the atmosphere on the environment. According to the Intergovernmental Panel on Climate Change (IPCC) (IPCC 2001), approximately 3/4 of the increase amount in atmospheric CO_2 is attributable to the combustion of fossil fuels, and it is acknowledged that fossil fuels will remain the leading source of energy for years to come, for both power generation and vehicle transportation. Therefore it's evident that the strategic importance of post combustion capture systems are required to avoid excess emissions from the ex-

isting fleet of power plants when considering the abundant sources of CO_2 emissions. Among all the post combustion capture technologies, gas absorption using alkanolamine solutions for CO_2 scrub is the most proven and tested capture process available on industrial scale. However, this process is energy-intensive for the regeneration of solvent and is also plagued by corrosion problems (Kikkinides et al. 1993), hence prompting the search for alternative technologies. One viable route is adsorption which, compared to other separation processes, is recognized to be attractive to complement or replace the current absorption technology due to its low energy requirement and operating flexibility (Aaron and Tsouris 2005; Yu et al. 2008; Audus 1997; Sjostrom and Krutka 2010).

Various cycle sequences of the PSA/VPSA process for CO_2 recovery are employed for different CO_2 concentration of the feed. When the feed concentration of CO_2 is higher than 25 %, high purity of CO_2 (over 99 %) can be easily produced by zeolite 13X at the recovery of 70 % using a single unit operated with 3-bed 7-step cycle (Chue et al. 1995). Most of the research in adsorption is focused on pressure/vacuum swing adsorption for separating CO_2 from flue gases (15 vol%) (Chue et al. 1995; Gomes and Yee 2002; Ko et al. 2003; Liu et al. 2011; Park et al. 2002; Takamura et al. 2001; Agarwal et al. 2010; Reynolds et al. 2008). Diagne et al. (1995) developed a new pressure swing adsorption process with intermediate feed inlet position operated with dual reflux. Their experimental results show that CO_2 could be concentrated from 20 to 90 % with feed pressure of 1.0 atm and desorption pressure of 0.12 atm. Reynolds et al. (2006) used high temperature PSA with potassium promoted hydrotalcite (HTlc) as adsorbent, and the purge/feed ratio, cycle step time and pressure ratio were studied and optimized. Xiao et al. (2008) achieved a CO_2 recovery of 90 % and purity of 80 % using zeolite 13X in a single three-bed VSA unit while processing the flue gas containing 12 % CO_2. Park et al. (2002) introduced two successive PSA units using 13X and made numerical analysis on the power consumption of the first PSA unit. Shen et al. (2012) employed two successive VPSA units, using activated carbon (AC) beads for CO_2 recovery, and a CO_2 purity of 95.3 % was obtained with 74.4 % recovery.

According to the large numbers of studies about the CO_2 recovery from low concentration flue gases (e.g., 15 % CO_2), it is difficult to achieve both high CO_2 purity and high recovery by single VPSA unit when capturing CO_2 from the flue gases at atmospheric pressure. If the flue gas is directly compressed from atmospheric pressure to a high pressure, high energy consumption is required due to the 85 % of N_2. Therefore, a process comprising two different VPSA units operating in series was designed in this work to concentrate CO_2 from flue gas to above 95 % with relative high recovery using 13XAPG. CO_2 was concentrated to about 60–80 % with the flue gas feeding at almost atmospheric pressure by the first VPSA unit. Then the product of the first unit was compressed and fed to the second VPSA unit, where CO_2 was further concentrated to above 95 % with a relatively high recovery. Moreover, single-column VPSA experiments with high feed concentration were performed to confirm the feasibility of two successive VPSA units.

2 Experiment setup and process description

VPSA experiments are performed on our laboratory unit. The lab VPSA unit contains three sections including gas mixture section, VPSA column section and the analytical section. The composition of simulated flue gas is adjusted by two mass-flow controllers (CS-200), while the effluents leaving the column are analyzed in the analytical section by a gas chromatograph and a CO_2 infrared online analyzer. The stainless steel adsorber is a tube without jacket filled with 13XAPG with inner diameter of 25 mm and wall thickness of 5 mm, operated at the ambient temperature. The VPSA equipment is connected to a computer where the individual gas flowrates and pressures at the inlet and outlet of the column are stored together with temperature measured in two different points of the column (0.07 and 0.28 m from the inlet). A full description of this laboratory unit has been done elsewhere (Wang et al. 2012).

The VPSA benchmark experiments are performed in a single column unit that operates under unsteady-state conditions to simulate the real operation of a column in a continuous multi-column VPSA. A four-step cycle including feed pressurization, adsorption, blowdown and purge with N_2 is employed for the single-column VPSA experiments. Some parameters relative to the column and adsorbent 13XAPG are summarized in Table 1.

3 Mathematical model

The theoretical model adopted to describe each of these individual columns had been described in the previous work (Wang et al. 2012), containing mass, energy and momentum balances among gas phase, solid phase, and column wall, including the following assumption (Da Silva 2003). Basic assumptions of the model is that the adsorbent is a solid with bidisperse pore structures, the pressure drop in the column is described by the Ergun equation and the mass transfer in macro-micropores can be described by a bi-LDF (Linear Driving Force) model. The gas phase exchanges mass and energy with the solid phase while only energy is exchanged with the column wall. The gas mixture interacts with the solid following the mass transfer governing equations including that between gas and solid interface, between gas

Table 1 Physical properties of zeolite 13X-APG and details of the adsorber column

Zeolite 13X-APG		Column packed with zeolite 13X-APG	
Pellet radius (average), m	0.00135	Column radius, m	0.0125
Pellet density, kg/m^3	1099.5	Column length, m	0.37
Pellet porosity	0.31	Column porosity	0.37
Crystal diameter, μm	1.5	Column density, kg/m^3	693
Adsorbent specific heat, J/(kg K)	920	Density of column wall, kg/m^3	8238
Tortuosity[a]	2.0	Column wall thickness, m	5×10^{-3}
		Wall heat capacity, J/(kg K)	500

[a]Estimated

Table 2 Fitting parameters of adsorption equilibrium and micropore diffusion parameters of pure CO_2 and N_2 in zeolite 13XAPG

Gas	K_0^i [kPa-1]	$(-\Delta H_i)$ [kJ/mol]	$q_{m,i}$ [mol/kg]	a_i	$D^0_{\mu,i}$ [m^2/s]	$-E_a$ [kJ/mol]
CO_2	5.249×10^{-7}	31.904	6.9293	3.3618	6.7×10^{-13}	11.7
N_2	4.390×10^{-7}	17.805	6.2707	3.7149	1.9×10^{-7}	10.8

and crystal inside the pellet and the thermodynamic equilibrium. Temperature inside the pellet is seen as uniform. The gas phase behaves as an ideal gas. Cross sectional area remains constant, and the void fraction is uniform along the column. No mass, heat, or velocity variations in the radial direction. Binary gas mixture of 15 % CO_2 and 85 % N_2 is assumed as the feed composition of the dry flue gas for the simulation. The multisite-Langmuir model is adopted to describe the adsorption equilibrium behavior of the mixture with parameters (Table 2) taken from pure component data previously reported (Wang et al. 2012).

The resulting model equations describing the adsorption bed in VPSA process are detailed in Table 3. Boundary and initial conditions used in this work can be found in Table 4. During the depressurization and blowdown steps, an exponential valve equation type is used in simulation. The fixed bed model involves several transport parameters that are calculated with frequently used correlations listed in Table 5 (Yang 1987; Wakao and Funazkri 1978; Poling et al. 2001; Wasch and Froment 1972; Ruthven 1984). The microspore diffusivities were measured in our previous work (Wang et al. 2012), as listed in Table 2. The heat transfer coefficient at the wall (hw) and external convective film transfer coefficient (U) were also previously fitted by the breakthrough curves. The values of hw and U are 32 W/(m^2 K^{-1}) and 12 W/(m^2 K^{-1}), respectively. The physical properties of the gases, like density, viscosity, and molar specific heat are calculated according to Poling et al. (2001), where the specific heat and the viscosity of the gas are estimated under the inlet conditions and taken as constant throughout the bed.

The modeling framework for multi-bed VPSA process is developed in gPROMS modeling environment (PSE Enterprise, UK) and reported in the previous work (Liu et al. 2011). Individual columns of the VPSA unit are connected by ancillary equipment to the columns: gas sources, valves, mass flow controllers, back-pressure regulators, and sinks. Detailed composite flowsheet of a two-column VPSA unit employed for process simulations of CO_2 removal from flue gases is shown in Fig. 1. The purge step is carried out with columns connected to each other, so that the purity of purge gas varies with time. Then the rinse gas comes from the product tank, and varies with time until CSS is achieved. Mass flow controllers delivers constant specified amount of gas during feed, purge and rinse steps; valves are considered as delay elements and can result in the disturbance to the flowrate with the distribution from time or severe pressure drop; headers are used to mimic the empty space in the top and bottom of each column for flow distribution and adsorbent accommodation; sources and sinks are destination devices that supply initial and final operating conditions.

The definition of the process parameters is:

$$\text{Purity}_{CO_2} = \frac{\int_0^{t_{blow}} C_{CO_2} u|_{Z=0} dt + \int_0^{t_{purge}} C_{CO_2} u|_{Z=0} dt}{\int_0^{t_{blow}} C_t u|_{Z=0} dt + \int_0^{t_{purge}} C_t u|_{Z=0} dt}$$

$$\text{Recovery}_{CO_2} = \frac{\int_0^{t_{blow}} C_{CO_2} u|_{Z=0} dt + \int_0^{t_{purge}} C_{CO_2} u|_{Z=0} dt}{\int_0^{t_{feed}+t_{press}} C_{CO_2} u|_{Z=0} dt}$$

$$\text{Productivity}_{CO_2} = \frac{(\int_0^{t_{blow}} C_{CO_2} u|_{Z=0} dt + \int_0^{t_{purge}} C_{CO_2} u|_{Z=0} dt) A}{t_{total} w_{adstotal}}$$

The power consumption of the VPSA processes is evaluated through simulations. The power consumption is calculated directly by the sum of the power for the blower and vacuum pump divided by the amount of CO_2 captured after cyclic steady state (CSS) is achieved. The theoretical definition of the power consumption is:

$$\text{Specific power}_{ave} = \frac{\int_0^{t_{press}+t_{feed}+t_{rinse}} W_{blower} dt + \int_0^{t_{blow}+t_{fpurge}} W_{vacuum} dt}{(\int_0^{t_{blow}} C_{CO_2} u|_{Z=0} dt + \int_0^{t_{purge}} C_{CO_2} u|_{Z=0} dt) A}$$

Table 3 Mathematical model of adsorber used for multibed VPSA processes for CO_2 capture from flue gas with zeolite 13XAPG

Adsorption isotherm for CO_2–N_2 mixture

Multi-site Langmuir isotherm:

$$\frac{q_i^*}{q_{\max,i}} = K_i P y_i \left[1 - \sum_i \left(\frac{q_i^*}{q_{\max,i}}\right)\right]^{a_i}$$

Van't Hoff equation:

$$K_i = K_i^0 \exp\left(-\frac{\Delta H_i}{R_g T_s}\right)$$

Equations for mass, energy, momentum balance

Component mass balance:

$$\varepsilon_c \frac{\partial C_i}{\partial t} = \varepsilon_c \frac{\partial}{\partial z}\left(D_{ax}\frac{\partial C_i}{\partial z}\right) - \frac{\partial (uC_i)}{\partial z} - (1-\varepsilon_c)a' k_{fi}\frac{1}{1+Bi_i}\left(C_i - \overline{C_i^p}\right)$$

Ergun equation:

$$\frac{\partial P}{\partial z} = -\frac{150\mu_g(1-\varepsilon_c)^2}{\varepsilon_c^3 d_p^2}u + \frac{1.75(1-\varepsilon_c)\rho_g}{\varepsilon_c^3 d_p}|u|u$$

LDF equation for the macropores:

$$\varepsilon_p \frac{\partial \overline{C_i^p}}{\partial t} + \rho_p \frac{\partial \langle \overline{q_i} \rangle}{\partial t} = \varepsilon_p \frac{15 D_{p,i}}{R_p^2}\frac{Bi_i}{1+Bi_i}\left(C_i - \overline{C_i^p}\right)$$

LDF equation for the micropores:

$$\frac{\partial \langle \overline{q_i} \rangle}{\partial t} = \frac{15 D_{\mu,i}}{r_c^2}\left(q_i^* - \langle \overline{q_i} \rangle\right)$$

Gas phase energy balance:

$$\varepsilon_c C_t C_v \frac{\partial T_g}{\partial t} = \frac{\partial}{\partial z}\left(\lambda \frac{\partial T_g}{\partial z}\right) - uC_t C_p \frac{\partial T_g}{\partial z} + \varepsilon_c R_g T_g \frac{\partial C_t}{\partial t} - (1-\varepsilon_c)a' h_f (T_g - T_s) - \frac{2h_w}{R_w}(T_g - T_w)$$

Solid phase energy balance:

$$(1-\varepsilon_c)\left[\varepsilon_p \sum_{i=1}^{n} \overline{C_i^p} C_{vi} + \rho_p \sum_{i=1}^{n} \langle \overline{q_i} \rangle C_{v,ads,i} + \rho_p C_{ps}\right]\frac{\partial T_s}{\partial t}$$
$$= (1-\varepsilon_c)\varepsilon_p R_g T_s \frac{\partial C_i}{\partial t} + \rho_b \sum_{i=1}^{n}(-\Delta H_i)\frac{\partial \langle \overline{q_i} \rangle}{\partial t} + (1-\varepsilon_c)a' h_f (T_g - T_s)$$

Wall energy balance:

$$\rho_w C_{pw}\frac{\partial T_w}{\partial t} = \alpha_w h_w (T_g - T_w) - \alpha_{wl} U (T_w - T_\infty)$$

with $\alpha_w = \frac{D_w}{e(D_w+e)}$, $\alpha_{wl} = \frac{1}{(D_w+e)\ln(\frac{D_w+e}{D_w})}$

The ideal gas behavior:

$$P = C_t R_g T_g C_t = \sum_{i=1}^{n} C_i$$

in which W_{blower} represents the power consumption of the blower during the pressurization and high pressure feed step while W_{vacuum} represents the power consumption in the blowdown and purge steps (using vacuum) that can be described by the following equations:

$$W_{blower} = \frac{\gamma}{\gamma - 1} R T_{feed}\left[\left(\frac{P_{feed}}{P_{atm}}\right)^{\frac{\gamma-1}{\gamma}} - 1\right] u(0)\pi R_c^2 \frac{P_{feed}}{R_g T_{feed}}$$

$$W_{vacuum} = \frac{\gamma}{\gamma - 1} R T_{blow}\left[\left(\frac{P_{atm}}{P_{blow}}\right)^{\frac{\gamma-1}{\gamma}} - 1\right] u(0)\pi R_c^2 \frac{P_{blow}}{R_g T_{blow}}$$

Since the mechanical efficiencies depend on the types of the vacuum pump and blower, system configuration, and manufacture, it is of little use to calculate the power consumption with a specific efficiency. Therefore, the idea power consumption given above is used to compare the process performance.

The mathematical models are solved using gPROMS software (PSE Enterprise, UK). The discretization method for the spatial domain in the column is the orthogonal collocation with finite elements method (OCFEM) with 50 intervals in the whole column. The set of ordinary and algebraic equations (ODAE) are integrated with the DASOLV solver which is based on backward-differentiation formulae (BDF). The solver uses a value of 1×10^{-5} for absolute tolerance.

Table 4 Boundary and initial conditions of the model equations

Boundary Conditions

Pressurization with feed:

$$-\frac{\varepsilon_c D_{ax}(i)}{u_i(0)}\frac{\partial C(i,0)}{\partial z}\bigg|_{z+} + C(i,0)|_{z-} - C(i,0)|_{z+} = 0$$

$$-\lambda\frac{\partial T(0)}{\partial z}\bigg|_{z+} + uC_tC_pT(0)|_{z-} - uC_tC_pT(0)|_{z+} = 0$$

$$P(0) = \frac{(P_{high} - P_{cycleend})}{t_{press}}\big(t - (N-1)t_{total}\big) + P_{cycleend}$$

$$u(L_c) = 0$$

$$\frac{\partial C(i,L_c)}{\partial z}\bigg|_{z-} = 0$$

$$\frac{\partial T(L_c)}{\partial z}\bigg|_{z-} = 0$$

Feed:

$$-\frac{\varepsilon_c D_{ax}(i)}{u(0)}\frac{\partial C(i,0)}{\partial z}\bigg|_{z+} + C(i,0)|_{z-} - C(i,0)|_{z+} = 0$$

$$-\lambda\frac{\partial T(0)}{\partial z}\bigg|_{z+} + uC_tC_pT(0)|_{z-} - uC_tC_pT(0)|_{z+} = 0$$

$$u(0)C(i,0)|_{z-} = u(0)C(i,0)|_{z+}$$

$$P(L_c) = P_{high}$$

$$\frac{\partial C(i,L_c)}{\partial z}\bigg|_{z-} = 0$$

$$\frac{\partial T(L_c)}{\partial z}\bigg|_{z-} = 0$$

Counter-current depressurization:

$$\frac{\partial C(i,0)}{\partial z}\bigg|_{z+} = 0$$

$$\frac{\partial T(0)}{\partial z}\bigg|_{z+} = 0$$

$$P(0) = (P_{high} - P_{blow})\big(1 - \exp\big(-\theta\big(t - (N-1)t_{total} - (t_{press} + t_{feed})\big)\big)\big) + P_{high}$$

$$\frac{\partial C(i,L_c)}{\partial z}\bigg|_{z-} = 0$$

$$\frac{\partial T(L_c)}{\partial z}\bigg|_{z-} = 0$$

$$u(L_c) = 0$$

Counter-current blowdown:

$$\frac{\partial C(i,0)}{\partial z}\bigg|_{z+} = 0$$

$$\frac{\partial T(0)}{\partial z}\bigg|_{z+} = 0$$

$$P(0) = (P_{high} - P_{blow})\big(1 - \exp\big(-\theta\big(t - (N-1)t_{total} - (t_{press} + t_{feed})\big)\big)\big) + P_{high}$$

$$\frac{\partial C(i,L_c)}{\partial z}\bigg|_{z-} = 0$$

$$\frac{\partial T(L_c)}{\partial z}\bigg|_{z-} = 0$$

$$u(L_c) = 0$$

Table 4 (*Continued*)

Counter-current purge:

$$P(0) = P_{exit}$$

$$\left.\frac{\partial C(i,0)}{\partial z}\right|_{z+} = 0$$

$$\left.\frac{\partial T(0)}{\partial z}\right|_{z+} = 0$$

$$-\frac{\varepsilon_c D_{ax}(i)}{u(0)}\left.\frac{\partial C(i,L_c)}{\partial z}\right|_{z-} + C(i,L_c)|_{z+} - C(i,L_c)|_{z-} = 0$$

$$-\lambda\left.\frac{\partial T(L_c)}{\partial z}\right|_{z-} + uC_tC_pT(L_c)|_{z+} - uC_tC_pT(L_c)|_{z-} = 0$$

$$u(L_c)C(i,L_c)|_{z-} = u(L_c)C(i,L_c)|_{z+}$$

Initial Conditions

$$\langle\overline{q_{CO_2}}\rangle(z) = 0, \qquad \langle\overline{q_{N_2}}\rangle(z) = q_{eq0,N_2}, \qquad T(z) = T_s(z) = T_w(z) = T_{feed}$$

$$C(z) = \overline{C_i^p} = \frac{P_{feed}y_{initial,i}}{R_gT_{feed}}$$

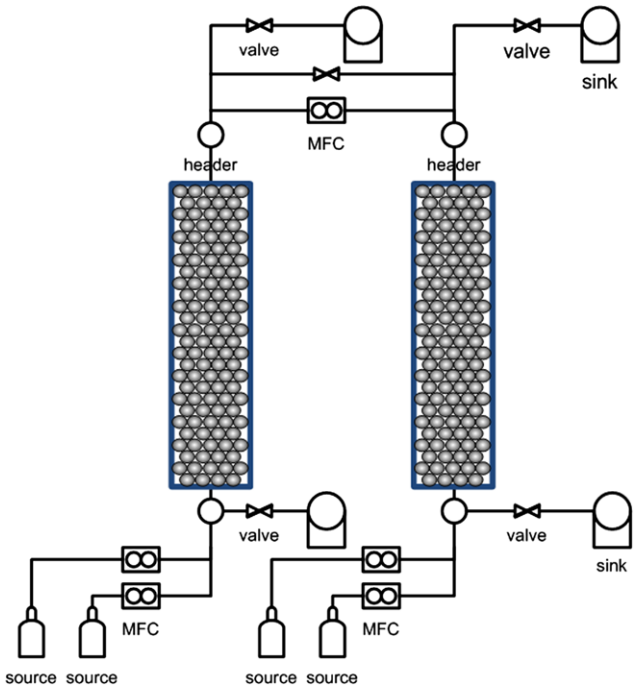

Fig. 1 Detailed composite flow sheet of a two-column VPSA unit employed for process simulations of CO_2 removal from flue gas

4 Results and discussion

4.1 Simulation of single VPSA unit with 3-bed 5-step cycle

Adsorption equilibrium and kinetics data of CO_2–N_2 mixtures on zeolite 13XAPG packed in a fixed bed were reported in our previous study (Wang et al. 2012), providing experimental validation to the mathematical model of the fixed bed. Before the numerical simulation of multi-bed VPSA for CO_2 capture, single-column VPSA experiments had been performed to validate the mathematical model and evaluate the viability. As reported in the previous work (Wang et al. 2012), through single-column VPSA experiments under a vacuum pressure of 10 kPa when processing a simulated flue gas containing 15 % CO_2 and 85 % N_2, a CO_2 purity of 60 % could be obtained with about 60 % recovery, far away from the 95 % purity limit for the following transportation and compression. It is very difficult to keep both the purity of CO_2 rich-stream and CO_2 recovery ratio from flue gas above 90 % by one column VPSA cycles. Although it can be noticed that good results will be obtained using very small pressure in the blowdown step due to the steepness of the isotherms of CO_2 on zeolite 13XAPG, 10 kPa is imposed in the blowdown and purge steps because of the trade off situation between high power consumption and desorption efficiency of CO_2.

The most important obstacle to obtain high CO_2 purity is the substantial amount of N_2 (gas phase and adsorbent voids) existing in the same steps that CO_2 is being recovered. For VPSA processes, usually a rinse step (i.e., heavy reflux) is included with part of purified carbon dioxide stream after the feed step to reduce the amount of N_2 from the gas phase and enhance the purity of CO_2 (Ruthven et al. 1994). Moreover, due to very difficult desorption resulting from the strong steepness of the CO_2 isotherms in the low-pressure range on 13XAPG, a light product purge step is required to obtain deeper bed regeneration and thus increase product recovery. However, it should be noted that the light product purge step can lead to a dilute CO_2 concentration. Consequently, a three-column VPSA unit is simulated with a five-step cycle described as follows:

Table 5 Calculation of transport parameters and physical properties of gases

Axial mass and heat dispersion coefficients

Wakao and Funazkri correlations ($3 < \mathrm{Re} < 10000$):

$$\frac{\varepsilon_c D_{ax}}{D_m} = 20 + 0.5 Sc\,\mathrm{Re}, \qquad \frac{\lambda}{k_g} = 7 + 0.5 \mathrm{Pr}\,\mathrm{Re}$$

The Schmidt, Reynold and Prandtl numbers were calculated as follows:

$$Sc = \frac{\mu_g}{\rho_g D_m}, \qquad \mathrm{Re} = \frac{\rho_g u d_p}{\mu_g}, \qquad \mathrm{Pr} = \frac{\mu_g C_{pgmass}}{k_g}$$

Mass and heat convective transfer coefficient

Wakao correlations:

$$Sh = 2.0 + 1.1\,\mathrm{Re}^{0.6}\,Sc^{1/3}, \qquad Nu = 2.0 + 1.1\,\mathrm{Re}^{0.6}\,\mathrm{Pr}^{1/3}$$

Sherwood number and Nusselt number were calculated as follows:

$$Sh = \frac{k_{fi} d_p}{D_m}, \qquad Nu = \frac{h_f d_p}{k_g}$$

Molecular diffusivity

The binary diffusivity was calculated using Chapman-Enskog equation:

$$D_{ij} = \frac{1.8809 \times 10^{-7} \sqrt{T^3 (\frac{1}{M_i} + \frac{1}{M_j})}}{P \sigma_{ij}^2 \Omega_{ij}},$$

where P is in bar, D_{ij} is in m^2/s.

$$\Omega_{ij} = 1.06036 \left(\frac{\varepsilon_{ij}}{kT}\right)^{0.15610} + 0.19300 e^{-0.47635 \frac{kT}{\varepsilon_{ij}}} + 1.03587 e^{-1.52996 \frac{kT}{\varepsilon_{ij}}} + 1.76474 e^{-3.89411 \frac{kT}{\varepsilon_{ij}}}$$

$$\sigma_{ij} = \frac{\sigma_i + \sigma_j}{2}, \qquad \varepsilon_{ij} = \sqrt{\varepsilon_i \varepsilon_j},$$

where σ_i (Å) and ε_i / k (K) are the characteristic Lennard-Jones length and energy of pure component i.

The molecular diffusivity of the gas relating to component i was calculated as follows:

$$D_{m,i} = \frac{1 - y_i}{\sum_{j=1, j \neq i}^{n} \frac{y_j}{D_{ij}}}$$

The molecular diffusivity of the mixture gas was calculated follows:

$$D_m = \sum_{i=1}^{n} y_i D_{m,i}$$

Knudsen diffusivity

Kauzmann correlation:

$$D_{k,i} = 9700 r_p \sqrt{\frac{T}{M_i}}$$

where r_p is in cm, $D_{k,i}$ is in cm^2/s.

Pore diffusivity

Bosanquet equation:

$$\frac{1}{D_{p,i}} = \tau_p \left(\frac{1}{D_{m,i}} + \frac{1}{D_{k,i}}\right)$$

Crystal diffusivity

Function of temperature described by:

$$D_{\mu,i} = D_{\mu,i}^0 \exp(-E_a / R_g T_s)$$

Heat capacity

Molar heat capacity at constant pressure of component i was calculated using:

$$\frac{C_{p,i}}{R} = A_0 + A_1 T + A_2 T^2 + A_3 T^3 + A_4 T^4$$

Table 5 (*Continued*)

Molar heat capacity at constant pressure of the gas mixture was calculated as:

$$C_p = \sum_{i=1}^{n} y_i C_{p,i}$$

The molar heat capacity at constant volume of in the ideal gas was calculated as:

$$C_v = C_p - R_g$$

The mass heat capacity at constant pressure of component i was calculated as:

$$C_{pgmass,i} = \frac{C_{p,i}}{M_i} \times 1000$$

The mass heat capacity at constant pressure of gas mixture was calculated as:

$$C_{pgmass} = \frac{\sum_{i=1}^{n} y_i C_{p,i}}{\sum_{i=1}^{n} y_i M_i} \times 1000$$

Viscosity

Viscosity of the pure gas was calculated according to the first order Chapman-Enskog equations:

$$\mu_i = 2.669 \times 10^{-6} \frac{(M_i T)^{0.5}}{\varepsilon_i \Omega_\mu}$$

where μ_i is in Pa s

$$\Omega_\mu = 1.16145\left(\frac{\varepsilon_i}{kT}\right)^{0.14874} + 0.52487e^{-0.7732\frac{kT}{\varepsilon_i}} + 2.16178e^{-2.43787\frac{kT}{\varepsilon_i}}$$

The viscosity of the gas mixture was calculated using Wilke method:

$$\mu_g = \sum_{i=1}^{n} \frac{y_i \mu_i}{\sum_{j=1}^{n} y_i \Phi_{ij}}$$

$$\Phi_{ij} = \left[8\left(1 + \frac{M_i}{M_j}\right)\right]^{-1/2}\left[1 + \sqrt{\frac{\mu_i}{\mu_j}}\left(\frac{M_i}{M_j}\right)^{-1/4}\right]^2$$

Density

$$\rho_g = \frac{P}{R_g T}\left(\sum_{i=1}^{n} y_i M_i\right) \Big/ 1000$$

where ρ_g is in (kg/m^3), P is in Pa.

Thermal conductivity

Wassiljewa method:

$$k_g = \sum_{i=1}^{n} \frac{y_i k_i}{\sum_{j=1}^{n} y_i A_{ij}}$$

$$A_{ij} = \Phi_{ij}$$

The thermal conductivity of the pure gas was calculated according to the following equations proposed by Eucken:

$$k_i = \left(C_{pgmass,i} + 1.25\frac{R_g}{M_i \times 10^{-3}}\right)\mu_i$$

where k_i is in W/m^2 K^{-1}.

Step 1 Pressurization (P). The pressure is increased from low pressure to a higher pressure with feed gas.

Step 2 Feed (FEED). The feed is kept at the high pressure, and CO_2 is selectively adsorbed.

Step 3 Rinse (RINSE). Part of the heavy product is recycled to the column before desorption. The product gas, which is already highly enriched in the heavy component, displaces the light component from the adsorbed phase near the feed end of the column and flushes it downstream toward the light-product end of the column.

Step 4 Blowdown (B). In this step, the most adsorbed components are partially removed from the adsorbent. The blowdown is carried out at lower pressure. In the simulation, a source is employed as the supplier for the rinse gas with settled pressure and flowrate controlled by a MFC. Then, if in the practical operation, the product gas is pumped into the storage tank

(a)first VPSA unit

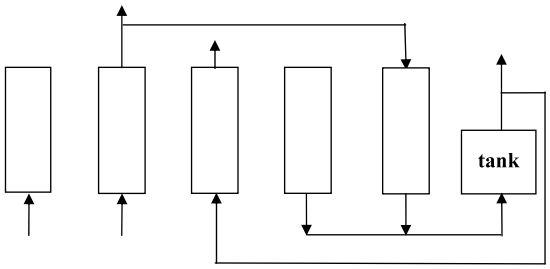

beds	steps									
1	FEED				R	B			PUR	P
2	B	PUR	P	FEED				R	B	
3	R	B				PUR	P	FEED		

(b)second VPSA unit

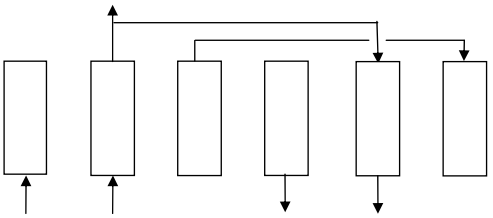

beds	steps									
1	P	FEED			EQ	B			PUR	EQ
2	B			PUR	EQ	P	FEED			EQ

Fig. 2 Schemes and cyclic configurations of the two successive VPSA units for CO_2 capture from flue gas using 13XAPG. Letters in the legend mean: B, blowdown; PUR, purge; R, rinse; EQ, pressure equalization; and P, pressurization

by vacuum pump and the pressure of the storage tank was controlled at an appropriate value.

Step 5 Purge (PURGE). A counter-current purge with inert gas exiting from the other column at the feed step is carried out. This step is also carried out at the lowest pressure of the system. The physical properties of the adsorbent and of the VPSA column used in the simulations are the same as the experimental unit listed in Table 1. The three-column scheme and cyclic configuration are shown in Fig. 2.

The operating conditions and step sequences employed in the simulations of this three-column VPSA cycle are detailed in Table 6 as well as the performance parameters obtained from simulations. The CO_2 concentration in the feed gas is 15 %, with adsorption pressure of 150 kPa, and rinse pressure of 100 kPa. The rinse gas is taken from gases obtained from the blowdown and purge steps (with various flowrates). As shown in Table 6, the CO_2 purity increases significantly with the rinse step (up to 80 %) keeping CO_2 recovery higher than 90 %. As shown in Table 6, the feed flow rate is changed from 0.8 to 3SLPM. When the feed flow rate increases from 0.8 to 3SLPM, CO_2 recovery decreases over 50 % while the purity increases less than 10 %. This means that the feed flow rate is more sensitive to the CO_2 recovery than to the product purity, making feed flow rate an important factor for designing the VPSA process for recovering CO_2 from the flue gas. The effects of rinse flow rate on the purity and recovery are also shown in Table 6. The flow rates of rinse gas are 0.3, 0.4, and 0.5SLPM. CO_2 recovery increases and the purity decreases with the decrease of rinse gas flowrate. Along with the increase of rinse gas flowrate, CO_2 concentration of the discharge stream may appears, because the rinse column is saturated with CO_2. Therefore, rinse flow rate is set as 0.3SLPM in all the other runs. It is clear from Table 6 that there is a trade-off situation among vacuum pressure, the purity, the recovery and the power consumption. Due to the limitation of the pump property for the deeper vacuum degree, the vacuum pressure is set at 10 kPa. It's observed that with such VPSA processes, over 85 % CO_2 can be recovered with purity ranging from 60–80 %, which is consistent with the results obtained in the literature (Liu et al. 2011;

Table 6 Process parameters and performances of single VPSA unit

Run	Q_{feed} [SLPM]	P_{low} [kPa]	Purity [%]	Recovery [%]	Q_{purge} [SLPM]	Q_{rinse} [SLPM]	W_1 [kJ/kg$_{CO_2}$]	Productivity [kg/(kg h)]
1	1	10	69.15	88.42	0.2	0.3	371.36	0.0361
2	2	10	75.92	55.66	0.2	0.3	456.52	0.0338
3	3	10	77.42	39.04	0.2	0.3	572.89	0.0357
4	0.8	10	65.38	98.92	0.2	0.3	361.70	0.0239
5	0.8	10	67.81	94.83	0.2	0.4	389.91	0.0226
6	0.8	10	70.33	91.40	0.2	0.5	418.46	0.0218
7	0.8	6	60.85	99.89	0.2	0.3	391.80	0.0257
8	0.8	15	65.68	84.84	0.2	0.3	353.71	0.0208
9	0.8	10	72.24	92.06	0.1	0.3	364.48	0.0223
10	0.8	10	59.19	99.35	0.3	0.3	364.10	0.0248

Note: For all the simulations, $yCO_2 = 15$ %, $T = 298$ K, $P_{feed} = 150k$

Table 7 Experimental conditions and performances of one column VPSA process for further concentrating CO_2 stream using zeolite 13XAPG

Runs	t_{feed} [s]	t_{press} [s]	t_{blow} [s]	t_{purge} [s]	yCO_2 [%]	Purity [%] (err(%))	Recovery [%] (err(%))	Productivity [kg/(kg h)] (err(%))
1	240	60	180	120	0.50	84.26(1.89)	77.73(0.44)	0.164(6.29)
2	235	65	180	120	0.60	84.44(0.63)	84.27(2.10)	0.177(4.32)
3	230	70	180	120	0.70	85.02(0.02)	91.47(0.03)	0.208(5.05)
4	225	75	180	120	0.80	87.07(0.11)	92.60(0.27)	0.209(2.96)
5	230	70	180	0	0.70	95.31(1.02)	81.38(0.63)	0.250(4.23)
6	235	65	180	0	0.60	94.18(0.83)	79.89(1.21)	0.233(5.61)

Note: For all the VPSA experiments, $T_{feed} = 300$ K, $P_{feed} = 134$ kPa, $F_{purge} = 0.15$ SLPM. err(%) = (Exp-Sim)/Exp*100%

Shen et al. 2012; Takamura et al. 2001; Park et al. 2002; Zhang and Webley 2008).

4.2 One-column VPSA experiment to further concentrate CO_2 rich stream

According to the previous simulation, it can be found that the single VPSA unit can concentrate CO_2 from 15 % to 60–80 % with recovery varied from 80 to 90 %. Therefore, one-column experiments with four-step Skarstrom-type cycle including co-current feed pressurization, feed, counter-current blowdown and counter-current N_2 purge and three-step cycle without purge are performed to validate the viability of the VPSA process with two successive units, where mixed gas with CO_2 concentrations varying from 60 to 80 % is prepared as the simulated product gas of the first VPSA unit and fed to the second VPSA unit. The properties of the columns used in the VPSA experiments are listed in Table 1. In the front four runs, the CO_2 amount in the feed step remained the same while the feed flowrate changed for the different feed concentration, in order to keep the handling capacity of CO_2 constant. The operating conditions and performances of experimental VPSA runs are listed in Table 7. Figure 3 shows experimental and simulated results the temperature profile of run 1(a) and the effect of different CO_2 feed concentrations on the second VPSA performance (b). The experimental and simulation results agree quite well. The product purity, the recovery and unit productivity increase with the increasing of feed CO_2 concentration. The purity and recovery are influenced by the amount of both the feed gas and the purge gas in the experiments. When comparing the four-step cycle and three-step cycle, with the feed concentration of 70 % it can be noted that the CO_2 purity was improved from 85 % to 95 % at the cost of the decrease of recovery, which means that the process with two successive VPSA units is viable.

4.3 Design of two successive VPSA units

Based on the three-column VPSA simulation results and one-column experimental study for further concentrating CO_2 stream, a process with two successive VPSA units comprising 3-bed 5-step cycle for the first VPSA unit and 2-bed 6-step cycle for the second VPSA unit operating in series is designed to concentrate CO_2 from flue gas to above 95 % with relative high recovery ratio and low specific power consumption. The main objective of the first VPSA unit, named as "front VPSA", is to obtain a high recovery (>90 %), and in the first unit, the CO_2 concentration is increased up to ~60 %. Then the CO_2 rich stream is compressed and further separated in the second VPSA unit,

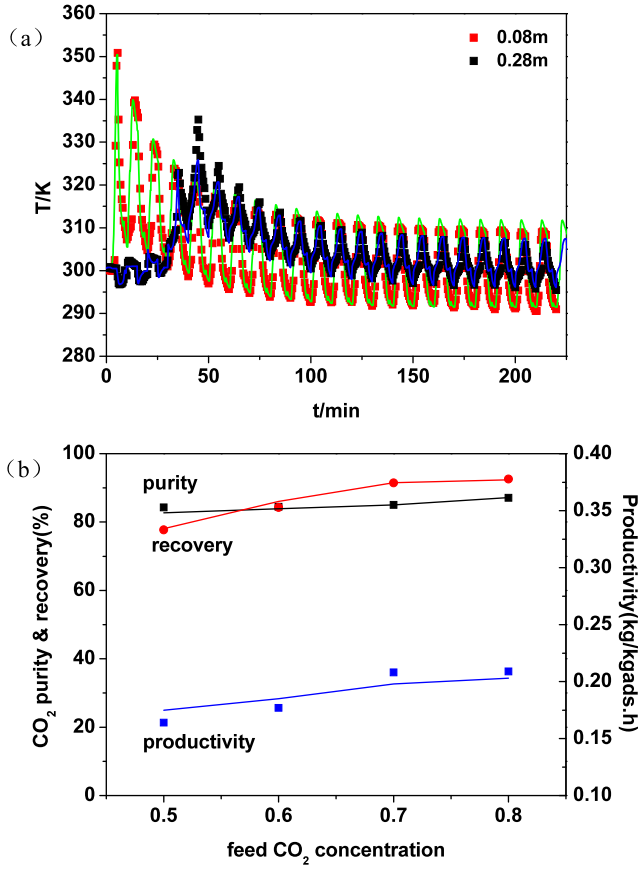

Fig. 3 (**a**) Experimental and simulated results of the temperature profile of the single column experiment. (**b**) Effects of the feed concentration on the purity, recovery and unit productivity of the single column experiments (*Solid lines*—theoretical model predictions, *solid points*—experimental values)

named as "tail VPSA". In steel industry, recovery and concentration of CO_2 to purity higher than 98 % is achieved using two PSA units in series (Park et al. 2002). It should be noted that the real flue gas contains extensive amount of water, which is strongly adsorbed in the adsorbent and difficult to be removed. In this work, we assume the water vapor is totally removed before the CO_2 capture process. Similar work has been performed by Ishibashi et al. (1996), and about 3 % curtailment of the required power consumption could be obtained.

Cyclic configuration of the second VPSA unit is also described in Fig. 2. A two-bed six-step VPSA cycle is used as the second unit including feed pressurization, adsorption, pressure equalization, blowdown, purge and pressure equalization. Pressure equalization is employed to save the mechanical energy. The purity and recovery of the overall two successive VPSA units are calculated by multiplying that of the first VPSA unit with that of the second VPSA unit. The total recovery will be less than that of first VPSA unit. Therefore, in order to satisfy the 95 % purity limit for the following transportation and compression as well as get higher CO_2 recovery from flue gas, Run 4 in Table 6 is selected as the operation conditions of the first VPSA unit for the following simulation of the two successive VPSA units. The simulations are carried out assuming non-isothermal and non-adiabatic behavior. As shown in Fig. 3(a), when processing high feed concentration, the temperature variation is large. The simulation should be conducted with proper consideration of the temperature effect. In our simulation, adsorption heat has been incorporated. Due to the inconstancy of the flowrate entering the second VPSA unit, a tank is associated to accumulate the gas coming from the first unit and provide a constant feed flowrate for the second VPSA unit. The dimensions and properties of the columns in the first VPSA unit are the same as that in the VPSA experiments, while the columns of the second VPSA unit are smaller than that of the first VPSA unit with bed length of 0.2 m and bed radius of 0.01 m. For the second VPSA unit, the step times, pressure and flowrate of each step are: $t_{press} = 100$ s (150, 250, 350 kPa); $t_{feed} = 300$ s (150, 250, 350 kPa); $t_{eq} = 30$ s; $t_{blow} = 300$ s (10, 15, 6 kPa); $t_{purge} = 100$ s ($Q = 0.01$ SLPM). The feed temperature and the ambient temperature is 298 K.

Simulations with different adsorption pressures, feed flowrates and vacuum pressures are performed to study the effects of these parameters on the performances of the integrated process with two successive VPSA units. The operating parameters and performances of the simulated integrated VPSA process are listed in Table 8. As shown in Table 8, the recovery and unit productivity increases while the CO_2 purity decreases with the level-up of the feed pressure of the second VPSA unit. When the adsorption pressure increases, more CO_2 will be adsorbed in the adsorbent resulting in the increase of recovery. However, as to the same amount of feed gas, due to the strong non-linearity of the CO_2 adsorption isotherms on 13XAPG and relatively linearity of the N_2 isotherms, more rise of the adsorption capacity of N_2 than CO_2 will be emerged when the adsorption pressure increases with more N_2 in the void, so that the purity of the product gas decreased. Whereas if the feed pressure reaches 250 and 350 kPa a compressor is required, so the power consumption increases significantly. Thus the optimal adsorption pressure should be determined by taking all these factors into consideration. Then the higher feed flowrate results in higher purity and productivity, with sharp drop of recovery, due to more CO_2 adsorbed and existed in the exhaust gas. Similar to the single VPSA unit discussed before, a trade-off situation also exists among vacuum pressure, the purity, the recovery and the power consumption. Although high product purity, recovery, and unit productivity can result from the decrease the vacuum pressure (from 15 to 6 kPa), the total power consumption increases obviously as more power consumption is required for the vacuum pump.

The mass balance of the two successive VPSA units, after CSS process (case 1) is reached, is presented in Fig. 4. Under

Table 8 Simulated results of two successive VPSA units for CO_2 capture from flue gases using zeolite 13XAPG

Case	First VPSA unit				Second VPSA unit				Integrated two successive VPSA units			
	Q_{feed} [SLPM]	P_{low} [kPa]	Purity [%]	Recovery [%]	P_{high} [kPa]	P_{low} [kPa]	Purity [%]	Recovery [%]	Purity [%]	Recovery [%]	W_{tot} [kJ/kg$_{CO_2}$]	Productivity [kg/(kg h)]
1	0.8	10	65.38	98.92	150	10	96.54	94.37	96.54	93.35	528.39	0.0312
2	0.8	10	65.38	98.92	250	10	94.35	96.68	94.35	95.64	573.94	0.0315
3	0.8	10	65.38	98.92	350	10	91.68	98.34	91.68	97.28	607.55	0.0314
4	1	10	69.15	88.42	150	10	97.59	91.92	97.59	81.28	533.2	0.0350
5	2	10	75.92	55.66	150	10	98.66	84.32	98.66	46.93	608.56	0.0422
6	0.8	6	60.85	99.89	150	6	96.61	97.99	96.61	97.88	594.01	0.0316
7	0.8	15	65.68	84.84	150	15	95.98	94.00	95.98	83.14	498.07	0.0273

Note: For all the simulations, $yCO_2 = 15$ %, $T = 298$ K

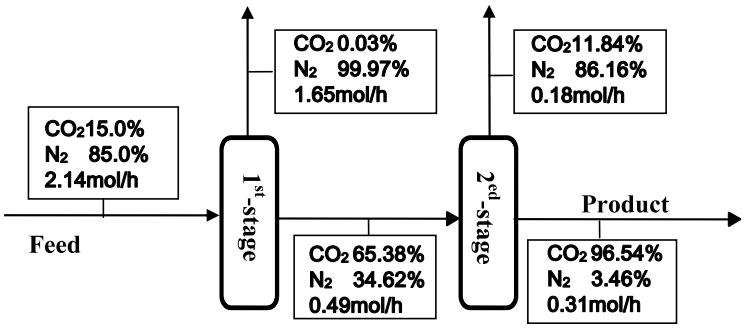

Fig. 4 Mass balance of the integrated VPSA process (case 1)

the conditions of vacuum pressure of 10 kPa, feed flowrate of 0.8 SLPM and adsorption pressure of 150 kPa, the performance of the integrated two successive VPSA units is: CO_2 recovery: 93.35 %, CO_2 purity: 96.54 %, unit productivity: 0.0312 kg$_{CO_2}$/(kg$_{ads}$ h), specific energy: 528.39 kJ/kg$_{CO_2}$. The exhaust gas from the outlet of the second unit contains relatively high CO_2 concentration of 11.84 % leading to the decrease of recovery. Therefore, this exhaust gas stream can be recycled to the feed stream in order to improve the capture recovery, only to slightly decrease the feed concentration.

The performances of various processes for CO_2 capture reported in the literatures are listed in Table 9 and compared with our VPSA process with two successive VPSA units. Park et al. (2002) introduced a two successive PSA process using 13X and made numerical analysis on the power consumption of the first PSA unit. The energy consumption was found to be in the range of 0.09–1.1 MJ/kg$_{CO_2}$ with purity ranging from 50 % to 70 % and recovery between 30 % and 90 % after one-stage PSA. Ishibashi et al. (1996) conducted a 2000 hours continuous PTSA operation in a 1000 Nm^3/h scale pilot plant, and a CO_2 purity of 99 % was obtained with 90 % recovery with power consumption of 560 kWh/t$_{CO_2}$. Shen et al. (2012) employed a two-stage vacuum pressure swing adsorption (VPSA) process, using activated carbon (AC) beads for CO_2 recovery and a CO_2 purity of 95.3 % was obtained with 74.4 % recovery. Cho et al. (2004) investigated two successive VPSA units with two beds for each stage packed with zeolite 13X, the CO_2 can be concentrated from 10.5 % to 99 % with a recovery of 80 %, while the experimental and theoretical power consumption was separately 2.31–2.79 MJ/kg$_{CO_2}$ and 513 kJ/kg$_{CO_2}$. The product purity and recovery in this work are a little higher, which mainly results from the high CO_2 capacity and selectivity of zeolite 13XAPG. The specific power consumption calculated in this work is in the same magnitude as the simulated results in their works. Though the experimental and simulated specific power consumption varies as a result of the different process configurations and operation conditions employed, the power consumption is lower than MEA absorption. Meanwhile because of the dependence of the size of the absorber and the amount of the adsorbents on the unit productivity, more efforts about optimization of the operation condition are still required to improve the productivity and reduce the power consumption of the whole capture system. Beside the indicator of the performance for various CO_2 capture process, the floor area, capital funds and operating costs including all the equipment, fixed general maintenance and labour costs should be taken into consideration for the actual CO_2 capture process. The CO_2 capture cost of two successive adsorption units may be higher than absorption, due to the high energy penalty for the compressor, as

Table 9 Comparison of performances of several CO_2 capture processes

Process	Adsorbent	$yCO_{2,feed}$ [%]	Desorption condition	Purity [%]	Recovery [%]	Power consumption	Literature	Result type
Two successive VPSA units	13XAPG	15	10 kPa	96.54	93.35	528.39 kJ/kg_{CO_2}	This work	Sim.
Two successive VPSA units	13XAPG	15	6 kPa	96.61	97.88	594.01 kJ/kg_{CO_2}	This work	Sim.
PTSA	CaX type zeolite	11.5	(0.05∼0.15) atm (323∼373) K	99	90	2016 kJ/kg_{CO_2}	(Ishibashi et al. 1996)	Exp.
FVPSA	13 X	15	(0.1∼0.7) atm	88.9	96.9	150.4 kJ/kg_{CO_2}	(Ko et al. 2003)	Sim.
PSA	13X	12.6	5–6 kPa	90–95	60–70	6–10 kW/TPDc	(Zhang and Webley 2008)	Exp.
Two-stage PSA	13 X	10.5	1st-stage: 6.67 kPa 2nd-stage: 13.34 kPa	99	80	513.2 kJ/kg_{CO_2}	(Cho et al. 2004)	Sim.
MEA absorption	–	13	–	>99	90	4–6 MJ/kg_{CO_2}	(Shen et al. 2012)	–
TSA	5A	10	423 K	≥94	75–85	(6120–6460) kJ/kg_{CO_2}	(Merel et al. 2008)	Exp.
Two-stage VPSA	AC beads	15	10 kPa	95.36	73.62	723.19 kJ/kg_{CO_2}	(Shen et al. 2012)	Sim.
Two-stage VPSA	AC beads	15	5 kPa	96.40	80.42	831.53 kJ/kg_{CO_2}	(Shen et al. 2012)	Sim.

Exp., experimental results; Sim., simulation results

while as low unit productivity resulting from large amount of adsorbent and adsorbent replacement costs.

5 Conclusions

In order to obtain a high CO_2 purity above 95 % with a relatively high recovery, the process with two successive VPSA units, comprising a first three-column unit and second two-column unit operating in series using zeolite 13XAPG as selective adsorbent to CO_2 recovery from flue gas, is developed through experiments and simulation. CO_2 is concentrated from 15 % to 60–80 % under almost atmospheric pressure in the first VPSA unit, and then further to above 95 % at the second VPSA unit. In order to achieve higher CO_2 purity, a three-bed five-step cycle is employed in the first VPSA unit, which includes feed pressurization, adsorption, rinse, blowdown and counter-current purge, and the influences for different operating parameters of this three-bed five-step cycle are investigated. It's noted that the CO_2 purity can't reach the purity limit (more than 95 %) for following transportation and compression when using a single VPSA unit packed with zeolite 13XAPG, so a process with two successive VPSA units is prompted. Before the integrated VPSA process simulation, single-column VPSA experiments are performed for CO_2/N_2 separation with high CO_2 feed concentration to evaluate the viability of the second VPSA unit. For the second VPSA unit, a cycle with feed pressurization, adsorption, pressure equalization, blowdown, purge and pressure equalization is adopted. A CO_2 purity of 96.54 % is obtained with recovery of 93.35 %. The total specific power consumption of the integrated VPSA process is 528.39 kJ/kg_{CO_2}, while the unit productivity is 0.0312 $kg_{CO_2}/(kg_{ads}\,h)$. These performance indicators are compared with other processes reported in the literatures. The operation conditions are still required to be optimized for improving the CO_2 capture capacity and reduce the power consumption of the whole capture system.

Acknowledgements The authors are grateful for the financial support of china 863 program (Grant No. 2008AA062302).

References

Aaron, D., Tsouris, C.: Separation of CO_2 from flue gas: a review. Sep. Purif. Technol. **40**(1), 321–348 (2005)

Agarwal, A., Biegler, L.T., Zitney, S.E.: A superstructure-based optimal synthesis of PSA cycles for post-combustion CO_2 capture. AIChE J. **56**(7), 1813–1828 (2010)

Audus, H.: Greenhouse gas mitigation technology: an overview of the CO_2 capture and sequestration studies and further activities of the IEA greenhouse gas R&D programme. Energy **22**(2), 217–221 (1997)

Cho, S.H., Park, J.H., Beum, H.T., Han, S.S., Kim, J.N.: A 2-stage PSA process for the recovery of CO_2 from flue gas and its power consumption. Stud. Surf. Sci. Catal. **153**, 405–410 (2004)

Chue, K.T., Kim, J.N., Yoo, Y.J., Cho, S.H., Yang, R.T.: Comparison of activated carbon and zeolite 13X for CO_2 recovery from flue gas by pressure swing adsorption. Ind. Eng. Chem. Res. **34**(2), 591–598 (1995)

Da Silva, F.A.: Cyclic adsorption processes: application to propane/propylene separation. Ph.D. thesis, University of Porto, Porto, Portugal (2003)

Diagne, D., Goto, M., Hirose, T.: Experimental study of simultaneous removal and concentration of CO_2 by an improved pressure

swing adsorption process. Energy Convers. Manag. **36**(6), 431–434 (1995)

Gomes, V.G., Yee, K.W.K.: Pressure swing adsorption for carbon dioxide sequestration from exhaust gases. Sep. Purif. Technol. **28**(2), 161–171 (2002)

IPCC: Climate Change 2001: Impacts, Adaptation and Vulnerability. Contribution of Working Group II to the Third Assessment Report of the Intergovernmental Panel on Climate Change. Cambridge University Press, Cambridge (2001)

Ishibashi, M., Ota, H., Akutsu, N., Umeda, S., Tajika, M., Izumi, J., Yasutake, A., Kabata, T., Kageyama, Y.: Technology for removing carbon dioxide from power plant flue gas by the physical adsorption method. Energy Convers. Manag. **37**(6), 929–933 (1996)

Kikkinides, E.S., Yang, R.T., Cho, S.H.: Concentration and recovery of carbon dioxide from flue gas by pressure swing adsorption. Ind. Eng. Chem. Res. **32**(11), 2714–2720 (1993)

Ko, D., Siriwardane, R., Biegler, L.T.: Optimization of a pressure-swing adsorption process using zeolite 13X for CO_2 sequestration. Ind. Eng. Chem. Res. **42**(2), 339–348 (2003)

Liu, Z., Grande, C.A., Li, P., Yu, J.G., Rodrigues, A.E.: Multi-bed vacuum pressure swing adsorption for carbon dioxide capture from flue gas. Sep. Purif. Technol. **81**(3), 307–317 (2011)

Merel, J., Clausse, M., Meunier, F.: Experimental investigation on CO_2 post combustion capture by indirect thermal swing adsorption using 13X and 5A zeolites. Ind. Eng. Chem. Res. **47**(1), 209–215 (2008)

Park, J.-H., Beum, H.-T., Kim, J.-N., Cho, S.-H.: Numerical analysis on the power consumption of the PSA process for recovering CO_2 from flue gas. Ind. Eng. Chem. Res. **41**(16), 4122–4131 (2002)

Poling, B.E., Prausnitz, J.M., O Connell, J.P.: The Properties of Gases and Liquids, 5th edn. McGraw-Hill, Boston (2001)

Reynolds, S.P., Ebner, A.D., Ritter, J.A.: Stripping PSA cycles for CO_2 recovery from flue gas at high temperature using a hydrotalcite-like adsorbent. Ind. Eng. Chem. Res. **45**(12), 4278–4294 (2006)

Reynolds, S.P., Mehrotra, A., Ebner, A.D., Ritter, J.A.: Heavy reflux PSA cycles for CO_2 recovery from flue gas: Part I. Performance evaluation. Adsorption **14**(2), 399–413 (2008)

Ruthven, D.M.: Principles of Adsorption and Adsorption Processes. Wiley, New York (1984)

Ruthven, D.M., Farooq, S., Knaebel, K.S.: Pressure Swing Adsorption. VCH Publishers, New York (1994)

Shen, C., Liu, Z., Li, P., Yu, J.: Two-stage VPSA process for CO_2 capture from flue gas using activated carbon beads. Ind. Eng. Chem. Res. **51**(13), 5011–5021 (2012)

Sjostrom, S., Krutka, H.: Evaluation of solid sorbents as a retrofit technology for CO_2 capture. Fuel **89**(6), 1298–1306 (2010)

Takamura, Y., Narita, S., Aoki, J., Hironaka, S., Uchida, S.: Evaluation of dual-bed pressure swing adsorption for CO_2 recovery from boiler exhaust gas. Sep. Purif. Technol. **24**(3), 519–528 (2001)

Wakao, N., Funazkri, T.: Effect of fluid dispersion coefficients on particle-to-fluid mass transfer coefficients in packed beds. Chem. Eng. Sci. **33**, 1375–1384 (1978)

Wang, L., Liu, Z., Li, P., Yu, J.G., Rodrigues, A.E.: Experimental and modeling investigation on post-combustion carbon dioxide capture using zeolite 13X-APG by hybrid VTSA process. Chem. Eng. J. **197**, 151–161 (2012)

Wasch, A.P.D., Froment, G.F.: Heat transfer in packed beds. Chem. Eng. Sci. **27**(3), 567–576 (1972)

Xiao, P., Zhang, J., Webley, P., Li, G., Singh, R., Todd, R.: Capture of CO_2 from flue gas streams with zeolite 13X by vacuum-pressure swing adsorption. Adsorption **14**(4), 575–582 (2008)

Yang, R.T.: Gas Separation by Adsorption Processes. Butterworths, Boston (1987)

Yu, K.M.K., Curcic, I., Gabriel, J., Tsang, S.C.E.: Recent advances in CO_2 capture and utilization. ChemSusChem **1**(11), 893–899 (2008)

Zhang, J., Webley, P.A.: Cycle development and design for CO_2 capture from flue gas by vacuum swing adsorption. Environ. Sci. Technol. **42**(2), 563–569 (2008)